

Supporting Information

Enhancing the Phosphorescence Decay Pathway of Cu(I) Emitters – The Role of Copper-Iodine Moiety

Giliandro Farias^[a], Cristian A.M. Salla^[b], Jéssica Toigo^[a], Luís Gustavo Teixeira Alves Duarte^[c], Adailton J. Bortoluzzi^[a], Edivandro Girotto^[a], Hugo Gallardo^[a], Teresa Dib Zambon Atvars^[c], Bernardo de Souza^{[a]*}, Ivan H. Bechtold^{[b]*}

^[a]Chemistry Department, Universidade Federal de Santa Catarina, 88040-900, Florianópolis, SC, Brazil

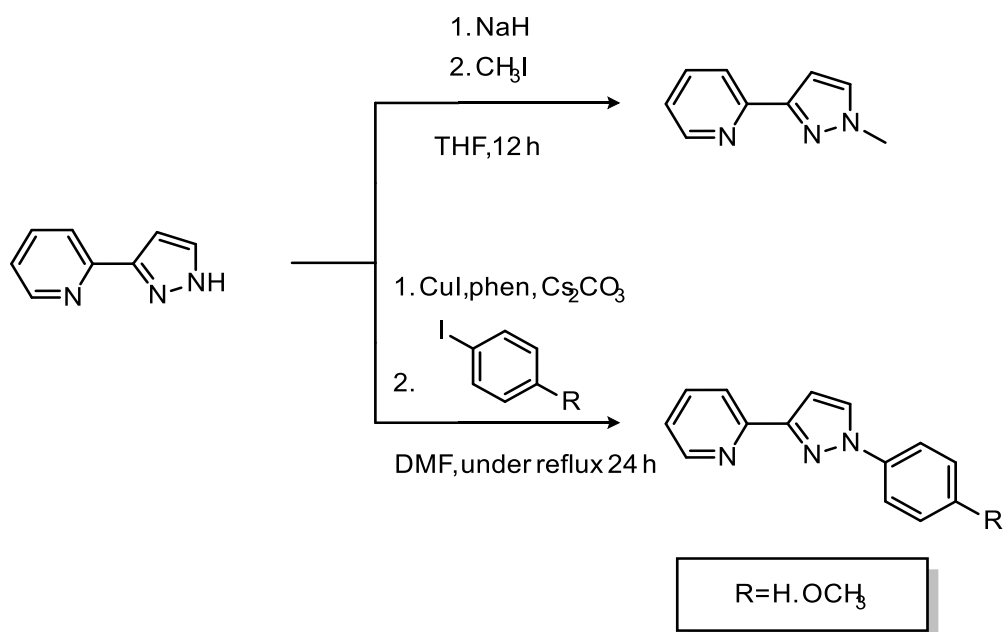
^[b]Physics Department, Universidade Federal de Santa Catarina, 88040-900, Florianópolis, SC, Brazil

^[c]Chemistry Department, Universidade Estadual de Campinas, 13083-970, Campinas, SP, Brazil

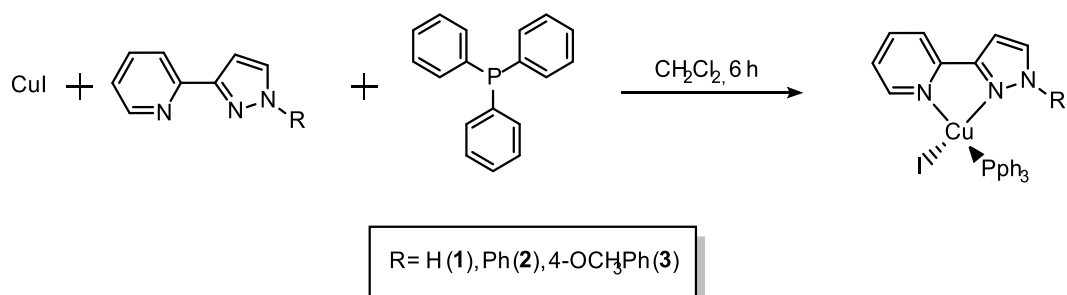
*Corresponding authors: bernadsz@gmail.com and ivan.bechtold@ufsc.br

- 1. Synthesis and Characterization**
- 2. NMR and IR Data**
- 3. Thermogravimetric Analyses and Cyclic Voltammetry Studies**
- 4. UV-Vis Absorption in Solution**
- 5. Theoretical Modeling**
- 6. X-Ray Crystallography**

1. Synthesis and Characterization



Scheme S1. Synthesis route to obtain the diimine ligands.



Scheme S2. Synthesis route to obtain complexes **1-3**.

2. NMR and IR Data

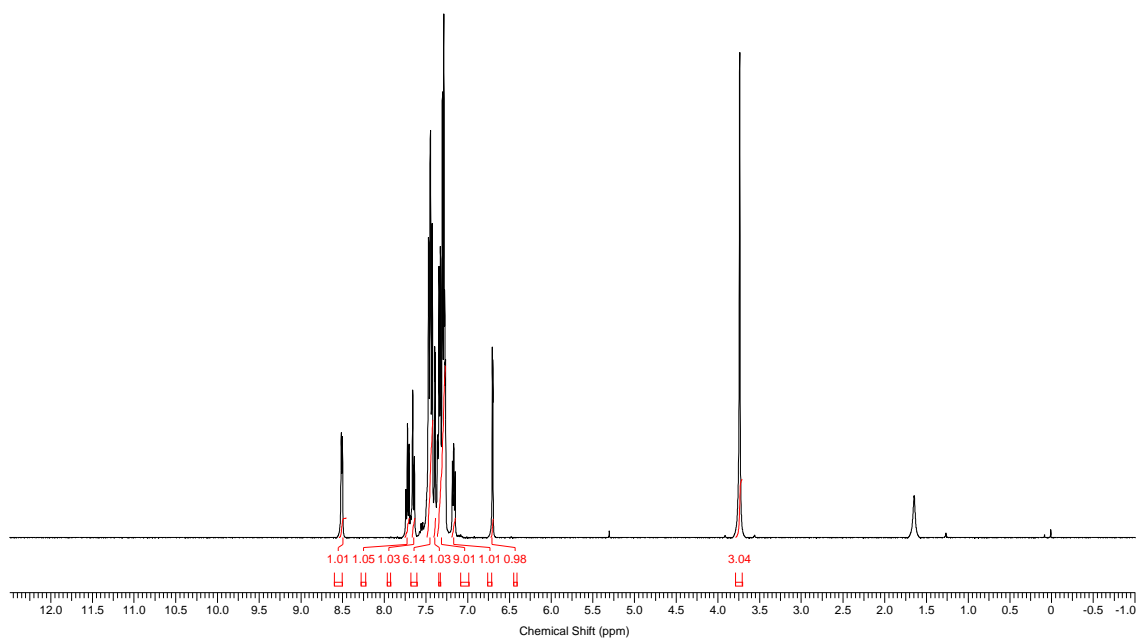


Figure S1. ¹H NMR spectrum (CDCl₃, 400 MHz) of compound **1**.

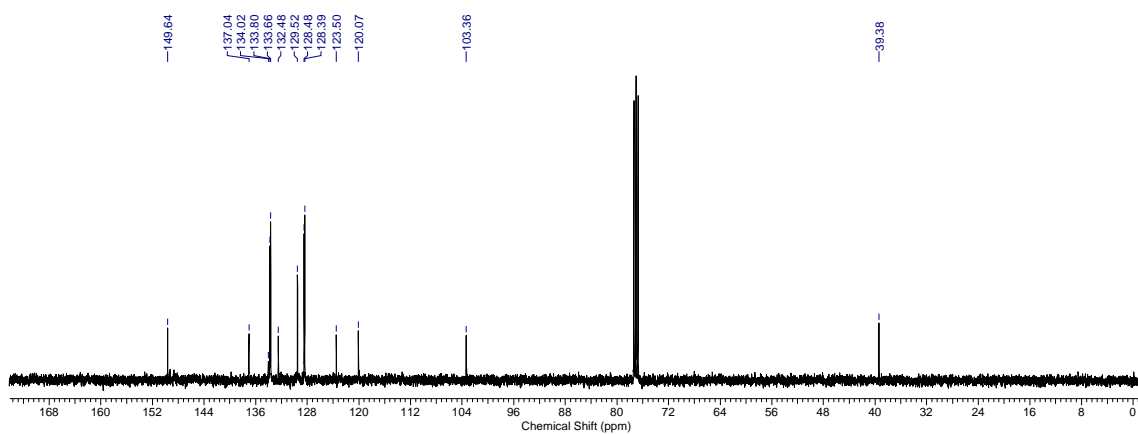


Figure S2. ¹³C NMR spectrum (CDCl₃, 100 MHz) of compound **1**.

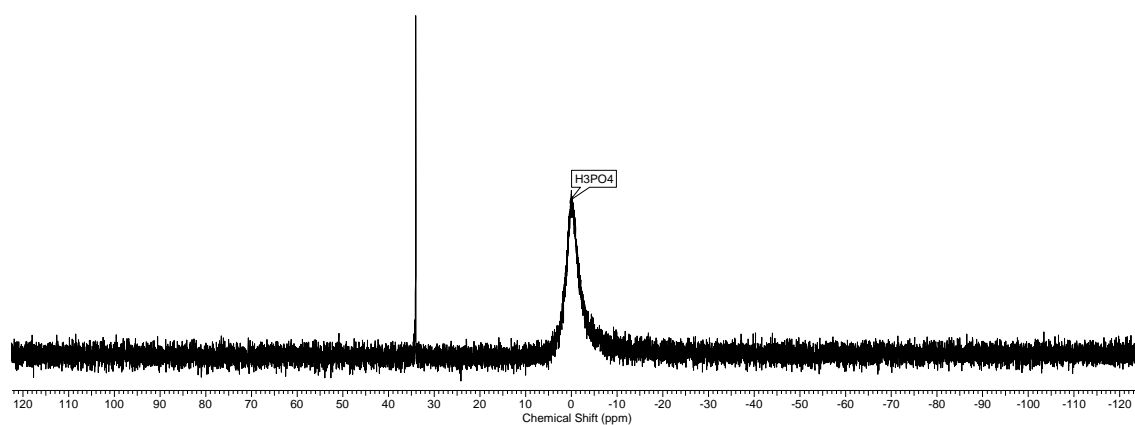


Figure S3. ³¹P NMR spectrum (CDCl₃, 162 MHz) of compound **1**.

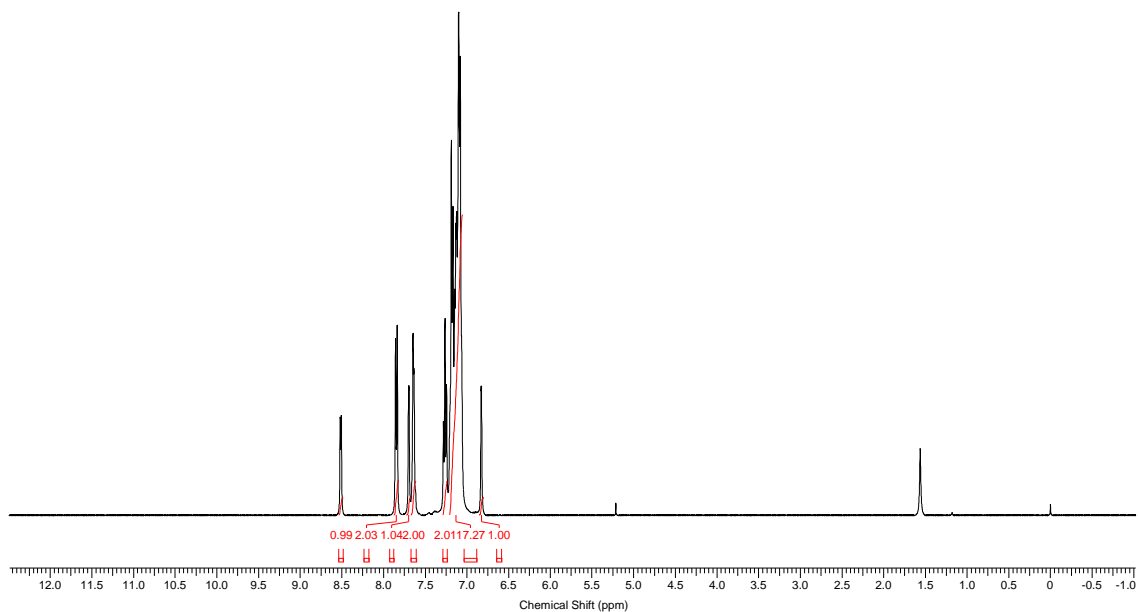


Figure S4. ^1H NMR spectrum (CDCl_3 , 400 MHz) of compound **2**.

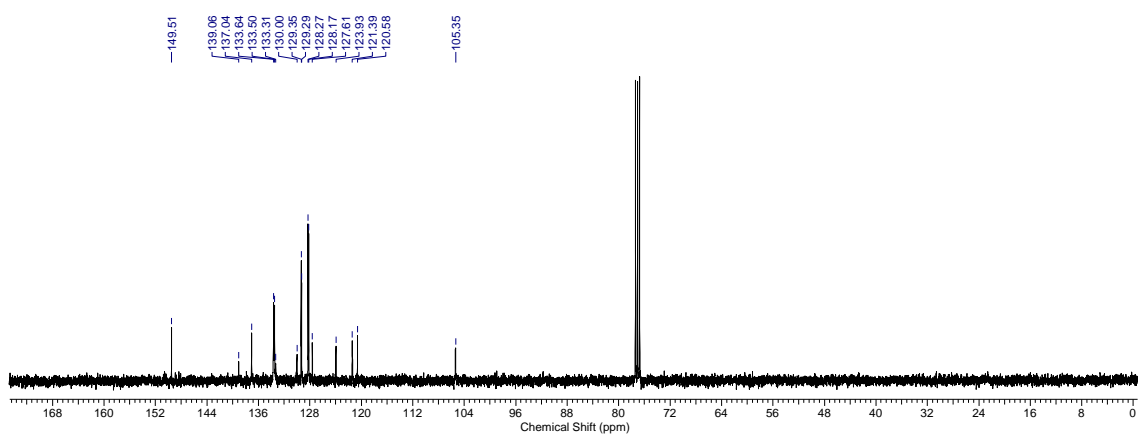


Figure S5. ^{13}C NMR spectrum (CDCl_3 , 100 MHz) of compound **2**.

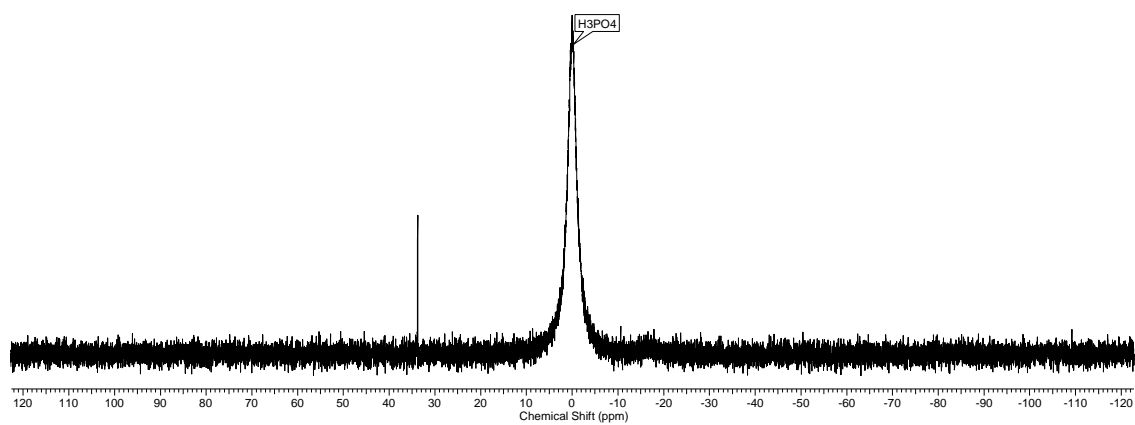


Figure S6. ^{31}P NMR spectrum (CDCl_3 , 162 MHz) of compound **2**.

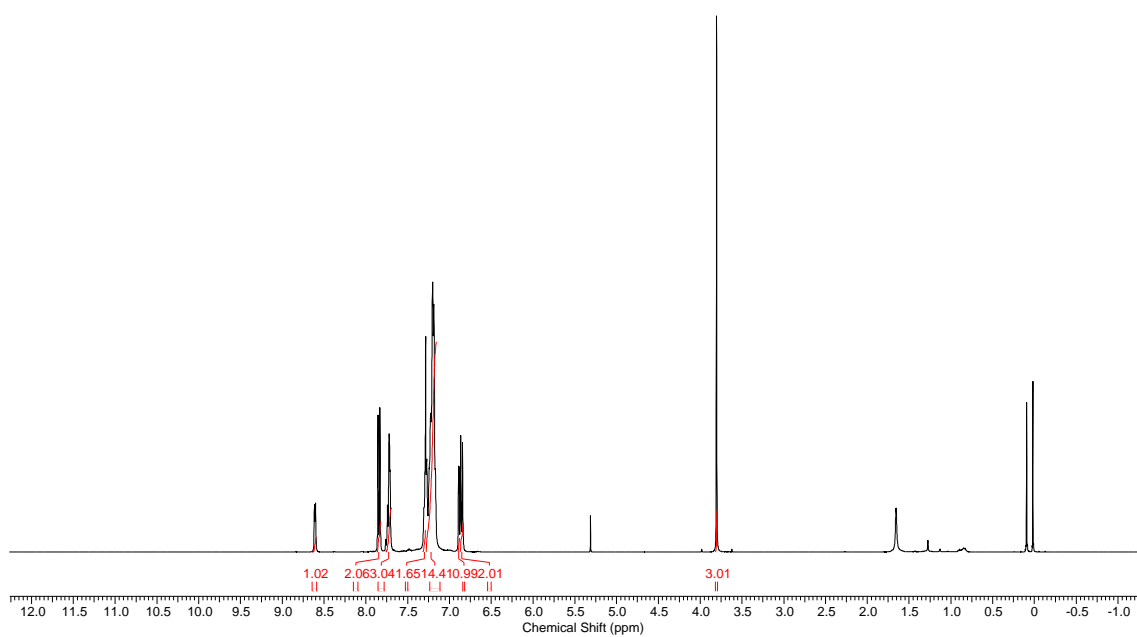


Figure S7. ^1H NMR spectrum (CDCl_3 , 400 MHz) of compound **3**.

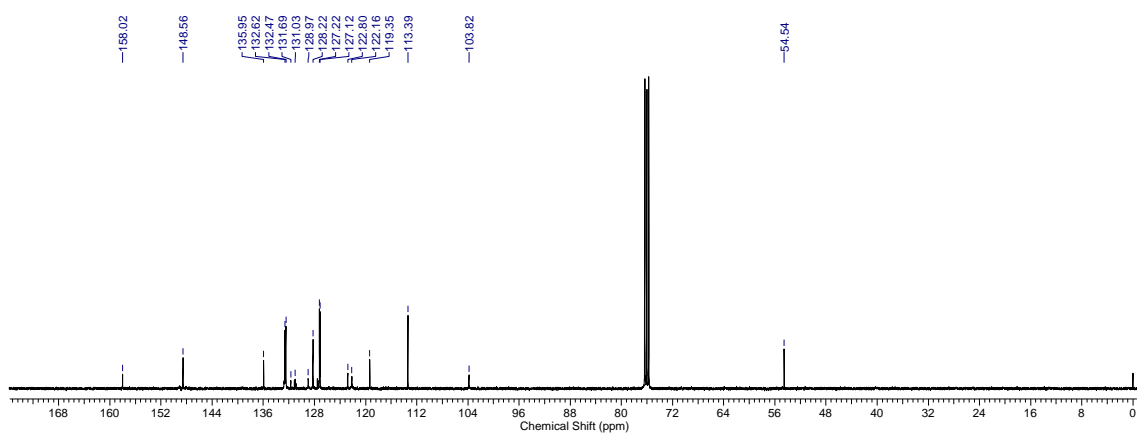


Figure S8. ^{13}C NMR spectrum (CDCl_3 , 100 MHz) of compound **3**.

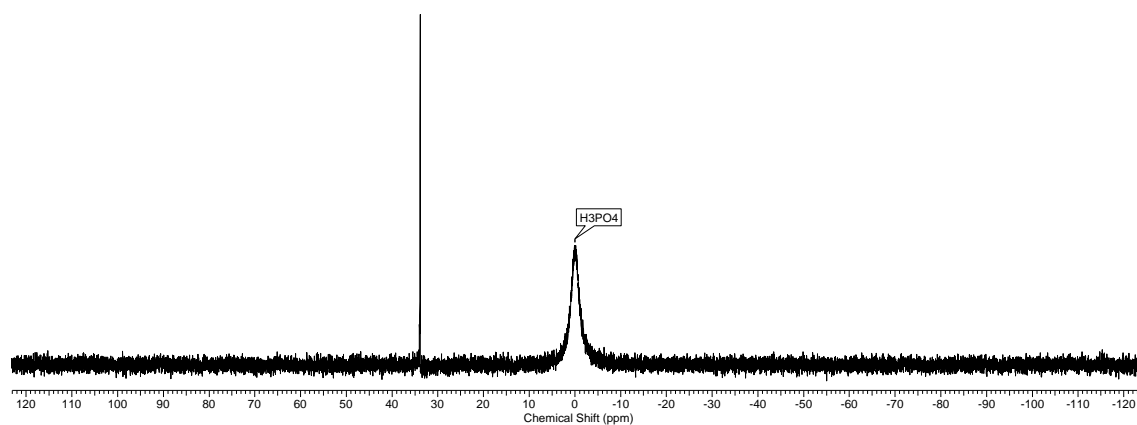


Figure S9. ^{13}C NMR spectrum (CDCl_3 , 162 MHz) of compound **3**.

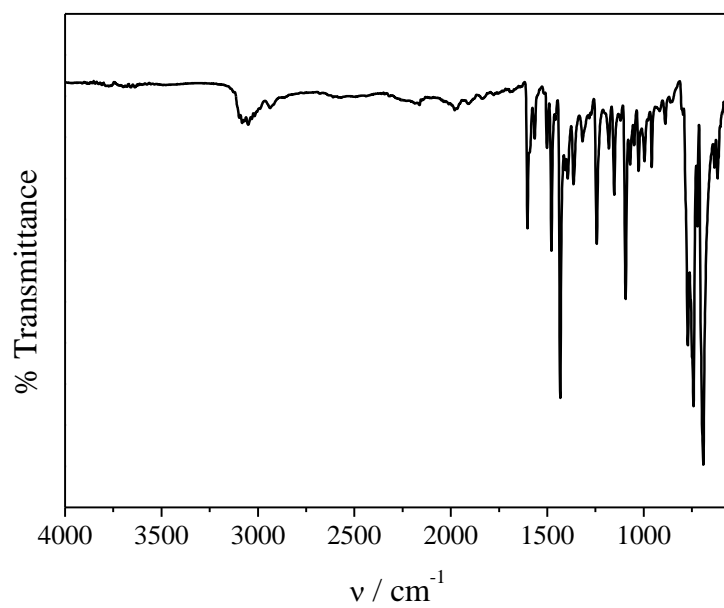


Figure S10. IR spectra of the complex **1**.

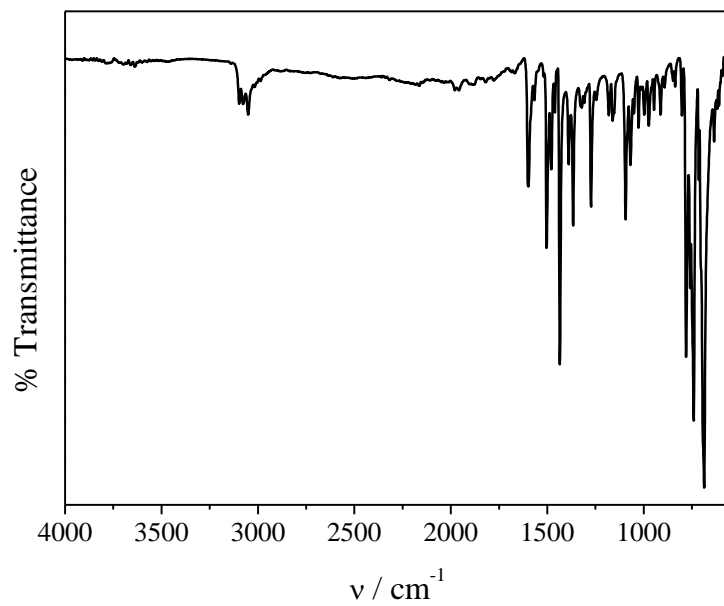


Figure S11. IR spectra of the complex **2**.

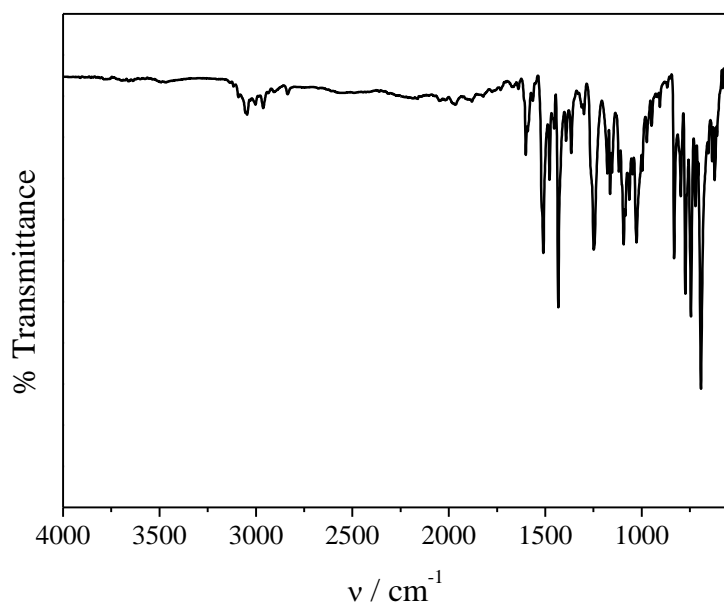


Figure S12. IR spectra of the complex **3**.

3. Thermogravimetric Analyses and Cyclic Voltammetry Studies

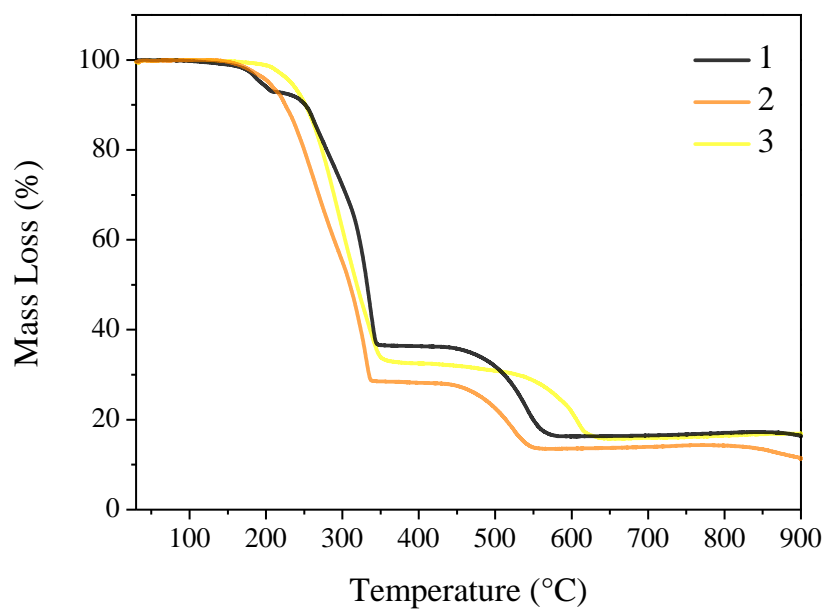


Figure S13. 1-3 thermogravimetric analysis (TGA) using a heating ramp of $10\text{ }^{\circ}\text{C min}^{-1}$ under nitrogen atmosphere.

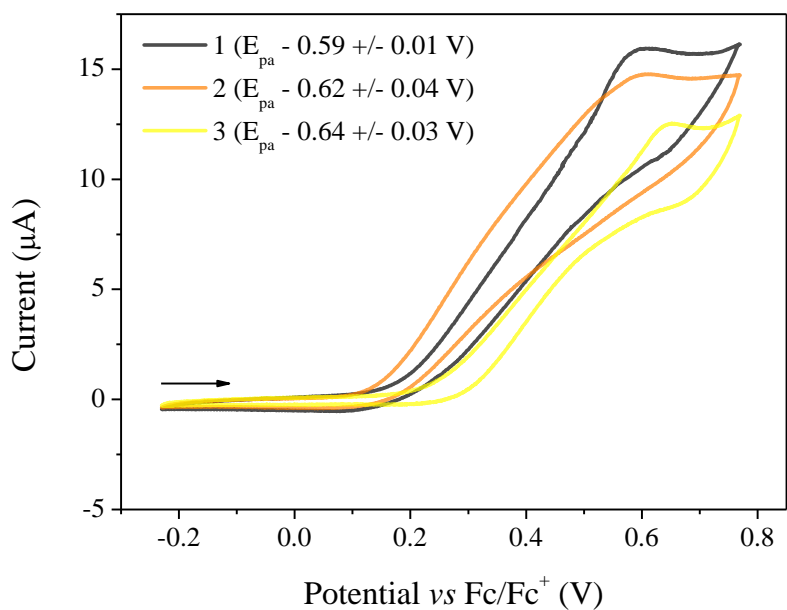


Figure S14. Cyclic voltammograms of the **1-3** complexes. Conditions: Working Electrode – Glassy Carbon; Reference Electrode - Ag/Ag⁺; Auxiliary Electrode - Platinum Wire; in dichloromethane solution, at 25 ± 1 ° C. The pair Fc/Fc⁺ was used as an internal standard.

4. UV-Vis Absorption in Solution

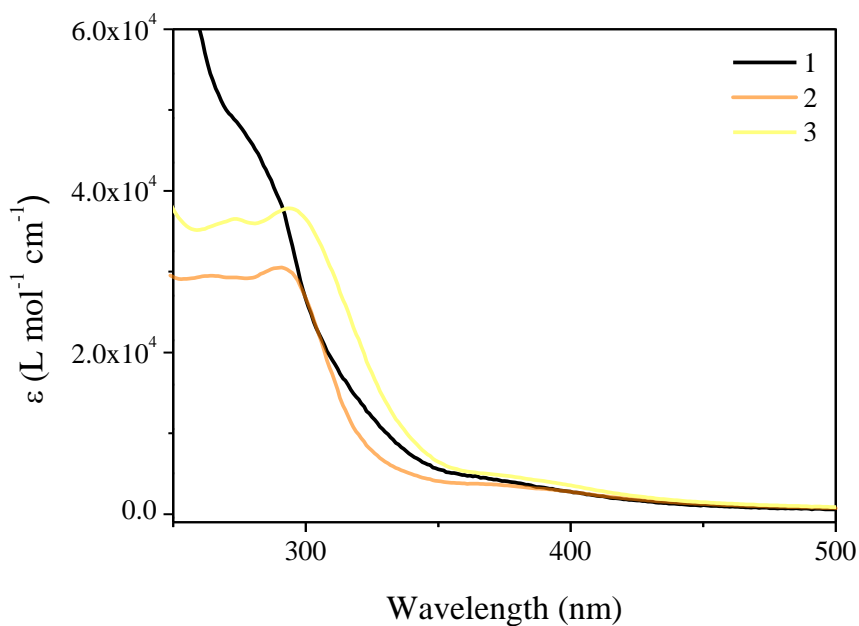


Figure S15. Optical absorption in dichloromethane solution 1.0×10^{-5} mol L⁻¹ of the Cu(I) complexes.

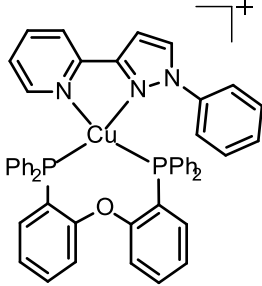
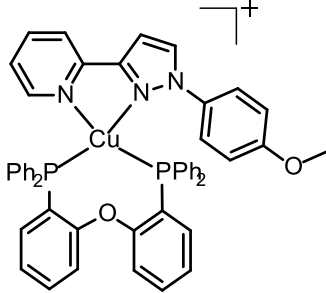
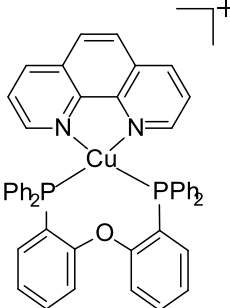
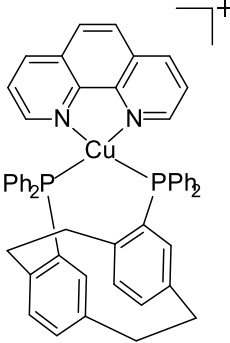
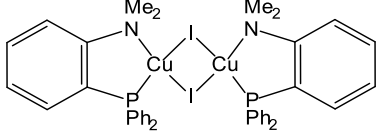
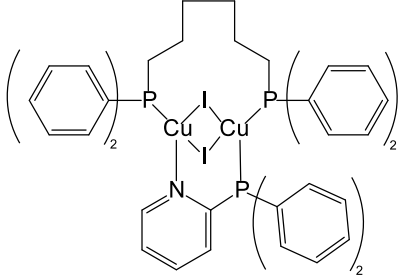
4	
5	
6	
7	
8	
9	

Figure S16. Molecular structure of the complexes discussed in Table 2 of the main text.

5. Theoretical Modeling

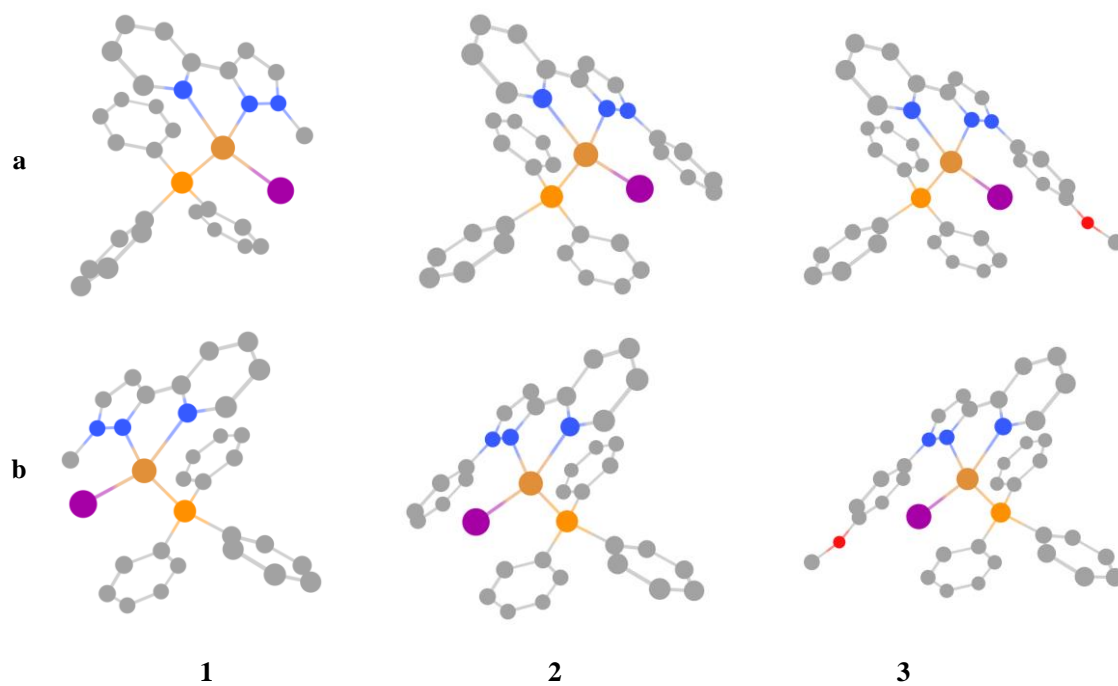


Figure S17. Optimized geometry for both isomers of complexes **1-3** obtained from DFT within PBE0/def2-TZVP(-f) and ZORA scalar-relativistic corrections level of theory.

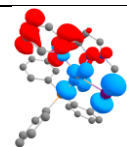
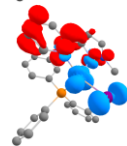
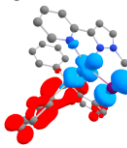
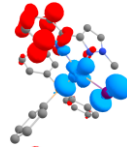
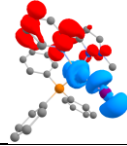
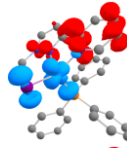
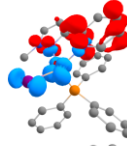
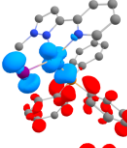
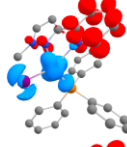
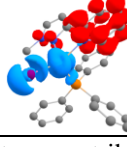
Table S1. Selected bond lengths (Å), bond angles (°) and τ_4 geometry index at optimized S_0 geometry for both isomers of complexes **1-3** within PBE0/def2-TZVP(-f) and ZORA scalar-relativistic corrections level of theory and experimentally determined by X-Ray diffractometry.

	1		2		3
	Exp	S₀ (1a/1b)	Exp	S₀ (2a/2b)	S₀ (3a/3b)
Cu(1)-P(1)	2.2061(12)	2.2047 2.2066	2.1968(11)	2.2029 2.2047	2.1925 2.2020
Cu(1)-I(1)	2.6065(7)	2.5214 2.5269	2.6127(6)	2.5286 2.5272	2.5566 2.5320
Cu(1)-N(1)	2.069(4)	2.0739 2.0748	2.062(3)	2.1349 2.1338	2.1093 2.1246
Cu(1)-N(12)	2.121(4)	2.1462 2.1506	2.116(3)	2.0935 2.0997	2.1097 2.0981
P(1)-Cu(1)-I(1)	118.85(4)	122.60 120.70	115.60(4)	121.02 121.10	120.30 120.73
N(1)-Cu(1)-P(1)	122.31(11)	105.66 107.40	120.58(9)	102.27 101.63	108.46 102.45
N(12)-Cu(1)-P(1)	111.64(11)	102.19 101.15	120.43(10)	108.76 107.50	120.34 107.32
N(1)-Cu(1)-N(12)	78.03(18)	77.00 77.03	78.32(13)	77.23 77.28	77.26 77.12
N(1)-Cu(1)-I(1)	106.35(12)	118.56 115.78	112.52(9)	123.69 123.66	118.65 123.22
N(12)-Cu(1)-I(1)	112.78(11)	121.17 126.02	102.98(10)	115.34 116.89	104.64 117.34
τ_4	0.843	0.824 0.803	0.844	0.818 0.817	0.847 0.823

Table S2. Selected bond lengths (Å), bond angles (°) and τ_4 geometry index at optimized T₁ geometry for both isomers of complexes **1-3** within PBE0/def2-TZVP(-f) and ZORA scalar-relativistic corrections level of theory and the root-mean-square deviation (RMSD) comparing the optimized T₁ and S₀ geometries.

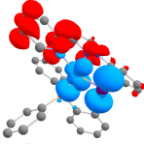
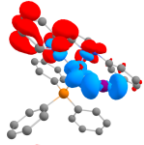
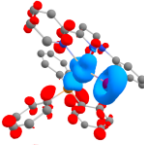
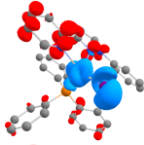
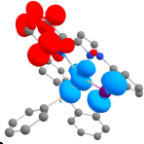
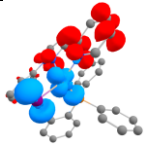
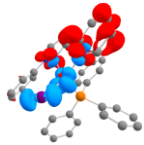

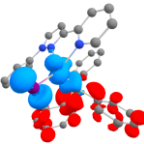
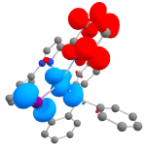
	1		2		3	
	a	b	a	b	a	b
Cu(1)-P(1)	2.3194	2.3264	2.3046	2.336	2.3093	2.3403
Cu(1)-I(1)	2.5759	2.5605	2.5015	2.5379	2.5071	2.5398
Cu(1)-N(1)	1.9732	1.9837	2.1123	1.9441	2.0888	1.9408
Cu(1)-N(12)	1.9504	1.9556	1.9311	1.9916	1.9291	1.9872
P(1)-Cu(1)-I(1)	96.60	96.36	105.39	96.52	96.60	95.22
N(1)-Cu(1)-P(1)	138.89	139.79	105.07	101.80	106.73	101.55
N(12)-Cu(1)-P(1)	98.88	98.16	94.79	132.02	94.83	134.91
N(1)-Cu(1)-N(12)	82.38	82.38	81.84	81.38	81.72	81.26
N(1)-Cu(1)-I(1)	105.00	105.70	123.21	149.51	121.77	148.85
N(12)-Cu(1)-I(1)	145.88	145.66	140.47	104.00	141.31	104.98
RMSD	1.0451	1.3850	0.5320	1.3418	0.5754	1.3818
τ_4	0.529	0.534	0.681	0.557	0.687	0.541

Table S3. Data for the TD-DFT excitations within PBE0/def2-TZVP(-f) and ZORA scalar-relativistic corrections level of theory for both isomers of complex **1**.

	State ^a	Energy			Configuration (%) ^b	TD-DFT Difference Densities ^c
		eV	nm	<i>f</i>		
1a	S ₁	3.098	400	0.0458	H → L (93)	
	S ₂	3.282	377	0.0020	H-1 → L (91)	
	S ₃	3.508	353	0.0122	H → L+1 (98)	
	S ₄	3.640	340	0.0016	H → L+2 (91)	
	S ₅	3.740	332	0.0292	H-2 → L (80)	
1b	S ₁	3.082	402	0.0392	H → L (93)	
	S ₂	3.238	383	0.0025	H-1 → L (91)	
	S ₃	3.482	356	0.0124	H → L+1 (98)	
	S ₄	3.671	338	0.0067	H → L+2 (62) H-2 → L (32)	
	S ₅	3.720	333	0.0342	H-2 → L (56) H → L+2 (35)	

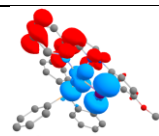
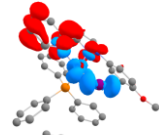
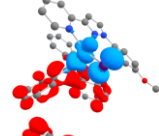
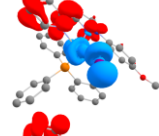
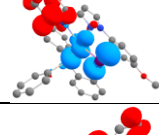
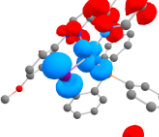
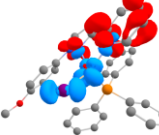
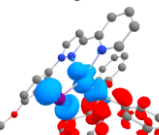
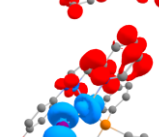
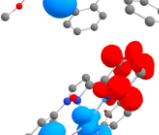
^a Vertical states taking S₀ geometry as the reference; ^b Transitions with high percentage contributions are shown in parenthesis; ^c For the TD-DFT difference densities between ground and specified excited-state hydrogen were omitted for clarity and blue indicates decreased and red indicates increased electronic density.

Table S4. Data for the TD-DFT excitations within PBE0/def2-TZVP(-f) and ZORA scalar-relativistic corrections level of theory for both isomers of complex **2**.

	State ^a	Energy			Configuration (%) ^b	TD-DFT Difference Densities ^c
		eV	nm	<i>f</i>		
2a	S ₁	2.969	417	0.0377	H → L (92)	
	S ₂	3.121	397	0.0124	H-1 → L (89)	
	S ₃	3.542	350	0.0125	H → L+1 (64) H-2 → L (30)	
	S ₄	3.553	349	0.0117	H → L+1 (34) H-2 → L (59)	
	S ₅	3.639	341	0.0087	H → L+2 (95)	
2b	S ₁	2.994	414	0.0439	H → L (92)	
	S ₂	3.115	398	0.0136	H-1 → L (88)	
	S ₃	3.548	349	0.0105	H-2 → L (88)	
	S ₄	3.581	346	0.0178	H → L+1 (96)	
	S ₅	3.647	340	0.0101	H → L+2 (96)	

^a Vertical states taking S₀ geometry as the reference; ^b Transitions with high percentage contributions are shown in parenthesis; ^c For the TD-DFT difference densities between ground and specified excited-state hydrogen were omitted for clarity and blue indicates decreased and red indicates increased electronic density.

Table S5. Data for the TD-DFT excitations within PBE0/def2-TZVP(-f) and ZORA scalar-relativistic corrections level of theory for both isomers of complex **3**.

	State ^a	Energy			Configuration (%) ^b	TD-DFT Difference Densities ^c
		eV	nm	<i>f</i>		
3a	S ₁	3.013	412	0.0428	H → L (93)	
	S ₂	3.154	393	0.0083	H-1 → L (90)	
	S ₃	3.523	352	0.0144	H → L+1 (97)	
	S ₄	3.587	345	0.0070	H-2 → L (80)	
	S ₅	3.655	339	0.0038	H → L+2 (94)	
3b	S ₁	3.030	409	0.0461	H → L (91)	
	S ₂	3.156	393	0.0127	H-1 → L (88)	
	S ₃	3.567	348	0.0173	H → L+1 (96)	
	S ₄	3.591	345	0.0071	H-2 → L(79)	
	S ₅	3.649	340	0.0056	H → L+2 (94)	

^a Vertical states taking S₀ geometry as the reference; ^b Transitions with high percentage contributions are shown in parenthesis; ^c For the TD-DFT difference densities between ground and specified excited-state hydrogen were omitted for clarity and blue indicates decreased and red indicates increased electronic density.

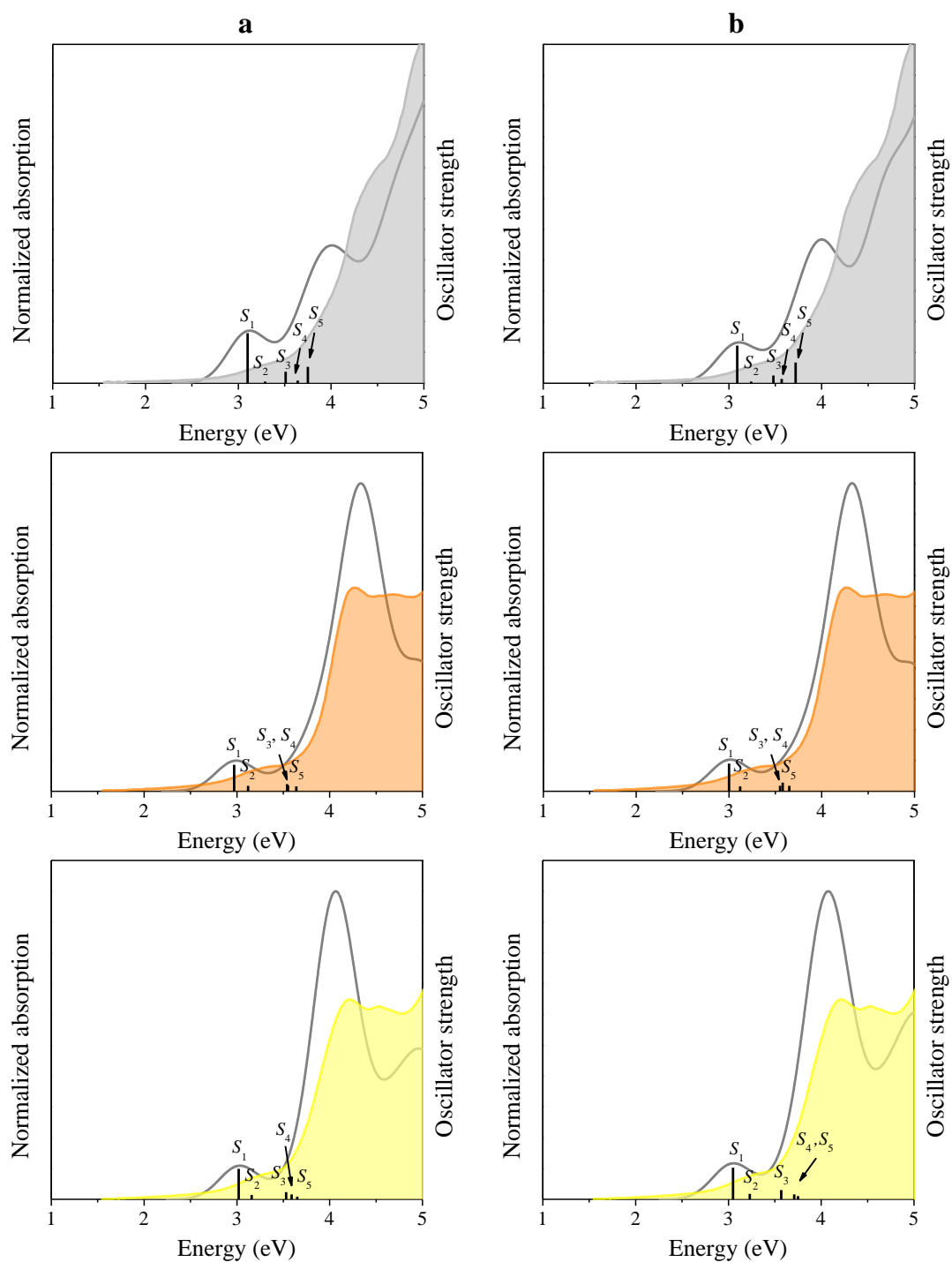
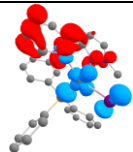
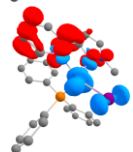
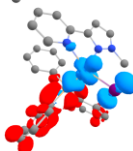
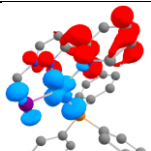
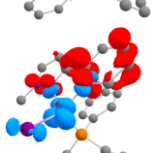
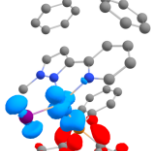


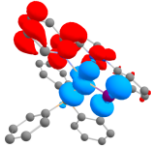
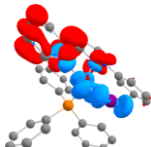
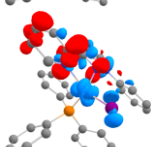
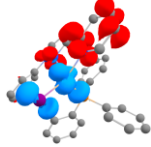
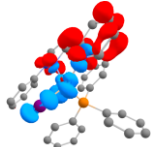
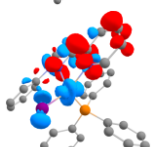
Figure S18. Experimental absorption spectra of **1-3** in CH_2Cl_2 (filled curves) and the theoretical absorption spectra (gray solid curves) for both respectively isomers **a** and **b** calculated within PBE0/def2-TZVP(-f) and ZORA scalar-relativistic corrections level of theory and convoluted with Gaussians of 0.50 eV width.

Table S6. Data for the SOC-TD-DFT triplet excitations within PBE0/def2-TZVP(-f) and ZORA scalar-relativistic corrections level of theory for both isomers of complex **1**.

	State ^a	Energy		f^b	Configuration (%) ^c	TD-DFT Difference Densities ^d
		eV	nm			
1a	T ₁	2.809	443	1.452×10^{-5}	H → L (90)	
	T ₂	3.131	397	1.219×10^{-2}	H-1 → L (83)	
	T ₃	3.382	367	1.931×10^{-5}	H → L+1 (85)	
1b	T ₁	2.832	440	1.772×10^{-5}	H → L (92)	
	T ₂	3.073	404	8.352×10^{-3}	H-1 → L (85)	
	T ₃	3.357	370	1.372×10^{-5}	H → L+1 (84)	

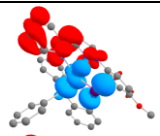
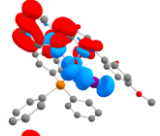
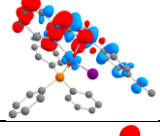
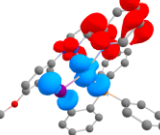
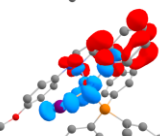
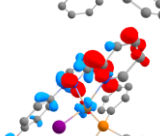
^a Vertical states taking S_0 geometry as the reference; ^b f for the triplet states are shown as an average of the substates x , y and z ; ^c Transitions with high percentage contributions are shown in parenthesis; ^d For the TD-DFT difference densities between ground and specified excited-state hydrogen were omitted for clarity and blue indicates decreased and red indicates increased electronic density.

Table S7. Data for the SOC-TD-DFT triplet excitations within PBE0/def2-TZVP(-f) and ZORA scalar-relativistic corrections level of theory for both isomers of complex **2**.

	State ^a	Energy		f^b	Configuration (%) ^c	TD-DFT Difference Densities ^d
		eV	nm			
2a	T ₁	2.709	461	2.515×10^{-5}	H → L (95)	
	T ₂	2.936	425	6.669×10^{-3}	H-1 → L (88)	
	T ₃	3.357	369	2.614×10^{-4}	H-5 → L (18) H-3 → L (28) H-2 → L (33)	
2b	T ₁	2.725	458	2.621×10^{-5}	H → L (95)	
	T ₂	2.932	426	4.914×10^{-3}	H-1 → L (88)	
	T ₃	3.349	370	3.318×10^{-4}	H-4 → L (12) H-3 → L (27) H-2 → L (34)	

^a Vertical states taking S_0 geometry as the reference; ^b f for the triplet states are shown as an average of the substates x, y and z; ^c Transitions with high percentage contributions are shown in parenthesis; ^d For the TD-DFT difference densities between ground and specified excited-state hydrogen were omitted for clarity and blue indicates decreased and red indicates increased electronic density.

Table S8. Data for the SOC-TD-DFT triplet excitations within PBE0/def2-TZVP(-f) and ZORA scalar-relativistic corrections level of theory for both isomers of complex **3**.

	State ^a	Energy		f^b	Configuration (%) ^c	TD-DFT Difference Densities ^d
		eV	nm			
3a	T ₁	2.749	454	8.595×10^{-6}	H → L (95)	
	T ₂	2.972	420	6.023×10^{-3}	H-1 → L (88)	
	T ₃	3.297	376	1.441×10^{-4}	H-2 → L (33) H-3 → L (37)	
3b	T ₁	2.760	452	1.068×10^{-5}	H → L (95)	
	T ₂	2.968	419	4.819×10^{-3}	H-1 → L (88)	
	T ₃	3.296	376	2.036×10^{-4}	H-2 → L (36) H-3 → L (35)	

^a Vertical states taking S₀ geometry as the reference; ^b f for the triplet states are shown as an average of the substates x, y and z; ^c Transitions with high percentage contributions are shown in parenthesis; ^d For the TD-DFT difference densities between ground and specified excited-state hydrogen were omitted for clarity and blue indicates decreased and red indicates increased electronic density.

Table S9. Comparison between theoretical prompt fluorescence rates and the experimental one determined from the Boltzmann type equation for **1-3**.

Complex	$ \langle I \mu F\rangle ^2$	$k_{\text{PF}}^{\text{THEO}}$ (s ⁻¹)	Complex	$k_{\text{PF}}^{\text{EXP}}$ (s ⁻¹)
1a	0.6151	3.91×10^7	1	1.88×10^6
1b	0.5134	3.21×10^7		
2a	0.5123	2.88×10^7	2	1.04×10^6
2b	0.5964	3.42×10^7		
3a	0.5767	3.37×10^7	3	3.33×10^6
3b	0.6179	3.89×10^7		

^a Determine using $k_{\text{PF}}^{\text{THEO}} = 2.136 \times 10^{10} \times |\langle I|\mu|F\rangle|^2 \times \Delta E(S_1)^3 \times \eta^2$, and setting η^2 as 2.016.

Table S10. Theoretical and experimental singlet and triplet energies and $\Delta E(S_1-T_1)$ for complexes **1-3**.

Theoretical	1a	2a	3a
S₁^a / eV	3.098	2.969	3.013
T₁^b / eV	2.809	2.709	2.749
$\Delta E(S_1-T_1)$^b / eV	0.289	0.260	0.264
Experimental	1	2	3
S₁^c / eV	2.58	2.57	2.55
T₁^c / eV	2.39	2.40	2.36
$\Delta E(S_1-T_1)$^d / eV	0.19	0.17	0.19

^a Vertical energy difference from TD-DFT; ^b Vertical energy difference from SOC-TD-DFT; ^c Experimental data obtained from the onset of the emission spectra at room temperature and 77 K; ^d $\Delta E(S_1-T_1)$ obtained from the difference between the S_1 and T_1 energies.

Table S11. Data of SOCME (in cm^{-1}) at optimized S_0 geometry within PBE0/def2-TZVP(-f) and ZORA scalar-relativistic corrections level of theory for both isomers of complexes **1-3**.

	1a	1b	2a	2b	3a	3b
$\langle \mathbf{T}_1 \mathbf{H}_{S_0} \mathbf{S}_0 \rangle^a$	46.63	44.44	26.59	30.14	21.33	23.75
$\langle \mathbf{T}_1 \mathbf{H}_{S_0} \mathbf{S}_1 \rangle^a$	38.81	20.74	73.62	77.49	51.60	72.08
$\langle \mathbf{T}_1 \mathbf{H}_{S_0} \mathbf{S}_2 \rangle^a$	399.10	416.55	392.40	385.63	378.67	380.72
$\langle \mathbf{T}_1 \mathbf{H}_{S_0} \mathbf{S}_3 \rangle^a$	16.44	18.76	201.53	359.48	28.81	49.63
$\langle \mathbf{T}_1 \mathbf{H}_{S_0} \mathbf{S}_4 \rangle^a$	53.73	156.60	274.98	58.98	319.30	330.84
$\langle \mathbf{T}_1 \mathbf{H}_{S_0} \mathbf{S}_5 \rangle^a$	253.99	217.04	53.57	41.18	53.15	53.33
$\langle \mathbf{T}_2 \mathbf{H}_{S_0} \mathbf{S}_0 \rangle^a$	87.21	85.62	58.63	56.32	59.72	58.84
$\langle \mathbf{T}_2 \mathbf{H}_{S_0} \mathbf{S}_1 \rangle^a$	471.44	479.65	455.35	456.28	445.90	448.44
$\langle \mathbf{T}_2 \mathbf{H}_{S_0} \mathbf{S}_2 \rangle^a$	30.45	37.92	135.65	152.00	105.16	134.16
$\langle \mathbf{T}_2 \mathbf{H}_{S_0} \mathbf{S}_3 \rangle^a$	11.36	14.40	233.27	405.14	36.13	53.70
$\langle \mathbf{T}_2 \mathbf{H}_{S_0} \mathbf{S}_4 \rangle^a$	108.61	226.35	306.34	59.27	371.63	376.73
$\langle \mathbf{T}_2 \mathbf{H}_{S_0} \mathbf{S}_5 \rangle^a$	355.76	263.30	37.09	35.08	34.78	36.55
$\langle \mathbf{T}_3 \mathbf{H}_{S_0} \mathbf{S}_0 \rangle^a$	28.84	39.48	36.76	39.12	24.61	26.17
$\langle \mathbf{T}_3 \mathbf{H}_{S_0} \mathbf{S}_1 \rangle^a$	37.96	27.72	281.33	302.85	159.38	172.11
$\langle \mathbf{T}_3 \mathbf{H}_{S_0} \mathbf{S}_2 \rangle^a$	15.81	17.46	262.97	273.97	136.97	149.58
$\langle \mathbf{T}_3 \mathbf{H}_{S_0} \mathbf{S}_3 \rangle^a$	15.47	11.34	16.37	28.90	3.43	1.37
$\langle \mathbf{T}_3 \mathbf{H}_{S_0} \mathbf{S}_4 \rangle^a$	15.31	13.81	23.68	7.52	26.09	24.85
$\langle \mathbf{T}_3 \mathbf{H}_{S_0} \mathbf{S}_5 \rangle^a$	36.96	22.96	37.03	37.18	22.10	22.61
$\Sigma \langle \mathbf{T}_{1-3} \hat{\mathbf{H}}_{S_0} \mathbf{S}_{1-5} \rangle$	1861.25	1944.65	2785.18	2697.44	2173.12	2306.71
$\Sigma \langle \mathbf{T}_{1-2} \hat{\mathbf{H}}_{S_0} \mathbf{S}_1 \rangle$	510.25	500.39	528.96	550.23	497.51	520.52

^a $\sqrt{\langle (\mathbf{S}_i | \mathbf{H}_{S_0} | \mathbf{T}_j)_{(MS=0,\pm 1)} \rangle^2}$ in the S_0 geometry.

Table S12. Data of SOCME (in cm⁻¹) at optimized T₁ geometry within PBE0/def2-TZVP(-f) and ZORA scalar-relativistic corrections level of theory for both isomers of complexes **1-3**.

	1a	1b	2a	2b	3a	3b
$\langle \mathbf{T}_1 \mathbf{H}_{\text{SO}} \mathbf{S}_0 \rangle^a$	70.30	72.38	51.71	64.36	52.21	64.08
$\langle \mathbf{T}_1 \mathbf{H}_{\text{SO}} \mathbf{S}_1 \rangle^a$	21.55	28.02	25.39	36.34	26.55	36.98
$\langle \mathbf{T}_1 \mathbf{H}_{\text{SO}} \mathbf{S}_2 \rangle^a$	27.64	24.34	387.51	369.59	373.18	363.15
$\langle \mathbf{T}_1 \mathbf{H}_{\text{SO}} \mathbf{S}_3 \rangle^a$	363.47	368.49	87.96	53.77	52.11	5.62
$\langle \mathbf{T}_1 \mathbf{H}_{\text{SO}} \mathbf{S}_4 \rangle^a$	99.13	13.11	237.73	241.35	203.75	62.83
$\langle \mathbf{T}_1 \mathbf{H}_{\text{SO}} \mathbf{S}_5 \rangle^a$	13.34	294.91	20.10	337.46	129.13	398.99
$\langle \mathbf{T}_2 \mathbf{H}_{\text{SO}} \mathbf{S}_0 \rangle^a$	169.08	143.28	94.82	119.64	94.73	113.75
$\langle \mathbf{T}_2 \mathbf{H}_{\text{SO}} \mathbf{S}_1 \rangle^a$	308.71	263.81	400.63	335.94	381.47	325.51
$\langle \mathbf{T}_2 \mathbf{H}_{\text{SO}} \mathbf{S}_2 \rangle^a$	24.19	12.20	149.85	189.64	152.04	226.06
$\langle \mathbf{T}_2 \mathbf{H}_{\text{SO}} \mathbf{S}_3 \rangle^a$	239.87	246.25	168.44	55.53	97.33	16.65
$\langle \mathbf{T}_2 \mathbf{H}_{\text{SO}} \mathbf{S}_4 \rangle^a$	120.97	42.83	452.24	482.58	414.09	68.89
$\langle \mathbf{T}_2 \mathbf{H}_{\text{SO}} \mathbf{S}_5 \rangle^a$	27.32	427.29	5.94	609.28	223.43	766.69
$\langle \mathbf{T}_3 \mathbf{H}_{\text{SO}} \mathbf{S}_0 \rangle^a$	62.40	116.83	25.44	41.45	24.25	48.02
$\langle \mathbf{T}_3 \mathbf{H}_{\text{SO}} \mathbf{S}_1 \rangle^a$	140.98	224.82	234.09	47.43	224.31	44.88
$\langle \mathbf{T}_3 \mathbf{H}_{\text{SO}} \mathbf{S}_2 \rangle^a$	17.36	18.95	375.01	36.67	321.51	35.18
$\langle \mathbf{T}_3 \mathbf{H}_{\text{SO}} \mathbf{S}_3 \rangle^a$	134.20	250.41	30.41	14.49	17.95	9.82
$\langle \mathbf{T}_3 \mathbf{H}_{\text{SO}} \mathbf{S}_4 \rangle^a$	55.81	21.38	150.35	64.40	129.98	7.99
$\langle \mathbf{T}_3 \mathbf{H}_{\text{SO}} \mathbf{S}_5 \rangle^a$	9.65	370.81	9.25	88.12	82.96	51.84
$\Sigma \langle \mathbf{T}_{1-3} \hat{\mathbf{H}}_{\text{SO}} \mathbf{S}_{1-5} \rangle$	1604.18	2607.62	2734.90	2962.58	2829.78	2421.07
$\Sigma \langle \mathbf{T}_{1-2} \hat{\mathbf{H}}_{\text{SO}} \mathbf{S}_1 \rangle$	385.03	291.83	426.02	372.28	408.02	362.48

^a $\sqrt{\langle (\mathbf{S}_i | \mathbf{H}_{\text{SO}} | \mathbf{T}_j)_{(\text{MS}=0,\pm 1)} \rangle^2}$ in the T₁ geometry.

Table S13. Comparison between theoretical phosphorescence rates and the experimental one obtained from the Boltzmann type equation for **1-3**.

Complex	T₁ (eV)^a	k_{Phosp}^{THEO} ^b (s⁻¹)	Complex	k_{Phosp}^{EXP} (s⁻¹)
1a	2.13	0.55 × 10 ⁴	1	0.97 × 10 ⁴
1b	2.16	0.63 × 10 ⁴		
2a	2.33	2.96 × 10 ⁴	2	1.26 × 10 ⁴
2b	2.14	1.77 × 10 ⁴		
3a	2.29	1.87 × 10 ⁴	3	0.99 × 10 ⁴
3b	2.10	1.45 × 10 ⁴		
Cu(phen)(POP)⁺	2.18	2.60 × 10 ³	Cu(phen)(POP)⁺	2.69 × 10 ³
Ir(bp)₂(acac)	1.87	1.56 × 10 ⁵	Ir(bp)₂(acac)	9.26 × 10 ⁴

^a Adiabatic energy; ^b Determined using $k_{\text{Phosp}} = \frac{\eta^3 E(T_j)^3}{1.5} \left\{ \sum_n \frac{\langle T_j | \hat{H}_{\text{SO}} | S_n \rangle}{E(S_n) - E(T_j)} \times \left(\frac{f_n}{E(S_n)} \right)^{\frac{1}{2}} \right\}^2$. The T₁ state adiabatic energy was used, η^3 set as 2.887 for the copper complexes and 2.785 for the iridium complex.

6. X-Ray Crystallography

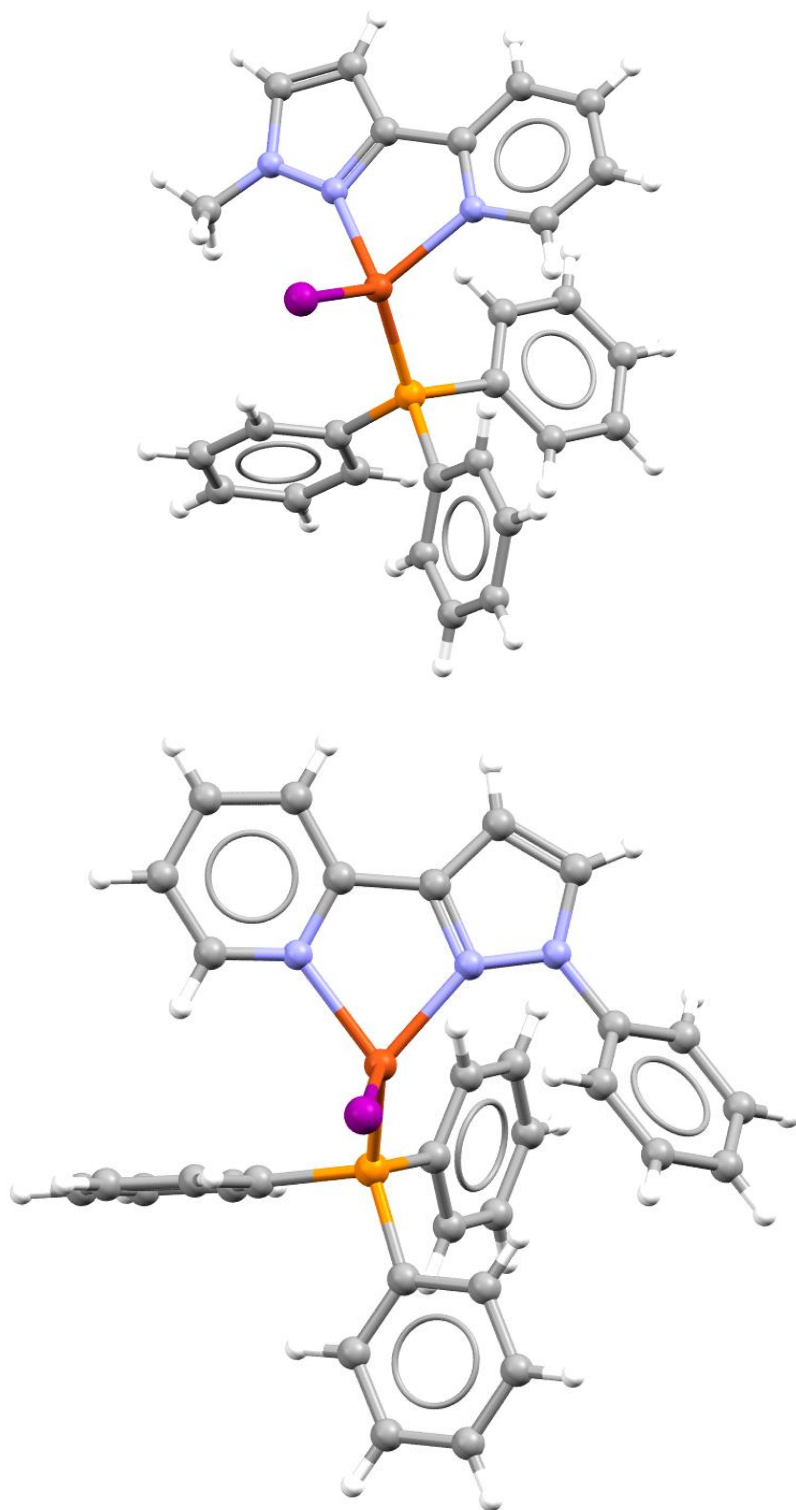


Figure S19. Molecular structure of complex **1** (top) and complex **2** (bottom).

Table S14. Crystal data and structure refinement for complex **1**.

Empirical formula	C ₂₇ H ₂₄ CuIN ₃ P [+ solvent]
Formula weight	611.90
Temperature	150(2) K
Wavelength	0.71073 Å
Crystal system	Monoclinic
Space group	P2 ₁ /n
Unit cell dimensions	a = 9.0460(10) Å b = 14.9018(17) Å c = 22.398(3) Å β = 98.696(2)°
Volume	2984.6(6) Å ³
Z	4
Density (calculated)	1.362 Mg/m ³
Absorption coefficient	1.837 mm ⁻¹
F(000)	1216
Crystal size	0.360 x 0.100 x 0.080 mm ³
Theta range for data collection	1.647 to 30.017°.
Index ranges	-12 ≤ h ≤ 10, -20 ≤ k ≤ 16, -31 ≤ l ≤ 31
Reflections collected	28144
Independent reflections	8616 [R(int) = 0.0444]
Completeness to theta = 25.242°	99.9 %
Absorption correction	Semi-empirical from equivalents
Max. and min. transmission	0.7460 and 0.6229
Refinement method	Full-matrix least-squares on F ²
Data / restraints / parameters	8616 / 0 / 299
Goodness-of-fit on F ²	1.015
Final R indices [I > 2σ(I)]	R1 = 0.0597, wR2 = 0.1307
R indices (all data)	R1 = 0.0984, wR2 = 0.1501
Extinction coefficient	n/a
Largest diff. peak and hole	3.235 and -3.073 e.Å ⁻³

Table S15. Bond lengths [Å] and angles [°] for complex **1**.

Cu(1)-N(1)	2.069(4)	P(1)-C(41)	1.823(5)
Cu(1)-N(12)	2.121(4)	C(21)-C(22)	1.394(6)
Cu(1)-P(1)	2.2061(12)	C(21)-C(26)	1.394(7)
Cu(1)-I(1)	2.6065(7)	C(22)-C(23)	1.388(7)
N(1)-N(2)	1.312(7)	C(23)-C(24)	1.377(9)
N(1)-C(5)	1.346(7)	C(24)-C(25)	1.373(9)
N(2)-C(6)	1.353(9)	C(25)-C(26)	1.394(8)
N(2)-C(3)	1.426(9)	C(31)-C(36)	1.384(7)
C(3)-C(4)	1.337(10)	C(31)-C(32)	1.387(6)
C(4)-C(5)	1.409(7)	C(32)-C(33)	1.391(8)
C(5)-C(11)	1.449(9)	C(33)-C(34)	1.380(8)
C(11)-N(12)	1.340(7)	C(34)-C(35)	1.384(7)
C(11)-C(16)	1.386(8)	C(35)-C(36)	1.390(7)
N(12)-C(13)	1.378(9)	C(41)-C(42)	1.385(7)
C(13)-C(14)	1.333(9)	C(41)-C(46)	1.387(7)
C(14)-C(15)	1.366(10)	C(42)-C(43)	1.399(8)
C(15)-C(16)	1.385(10)	C(43)-C(44)	1.370(10)
P(1)-C(31)	1.820(5)	C(44)-C(45)	1.378(10)
P(1)-C(21)	1.821(5)	C(45)-C(46)	1.385(8)
N(1)-Cu(1)-N(12)	78.03(18)	C(3)-C(4)-C(5)	105.7(6)
N(1)-Cu(1)-P(1)	122.31(11)	N(1)-C(5)-C(4)	112.1(6)
N(12)-Cu(1)-P(1)	111.64(11)	N(1)-C(5)-C(11)	117.8(5)
N(1)-Cu(1)-I(1)	106.35(12)	C(4)-C(5)-C(11)	130.0(5)
N(12)-Cu(1)-I(1)	112.78(11)	N(12)-C(11)-C(16)	120.4(6)
P(1)-Cu(1)-I(1)	118.85(4)	N(12)-C(11)-C(5)	114.7(5)
N(2)-N(1)-C(5)	104.2(5)	C(16)-C(11)-C(5)	124.8(5)
N(2)-N(1)-Cu(1)	141.2(4)	C(11)-N(12)-C(13)	116.9(5)
C(5)-N(1)-Cu(1)	114.6(4)	C(11)-N(12)-Cu(1)	114.7(4)
N(1)-N(2)-C(6)	119.5(6)	C(13)-N(12)-Cu(1)	128.3(4)
N(1)-N(2)-C(3)	112.5(6)	C(14)-C(13)-N(12)	127.2(8)
C(6)-N(2)-C(3)	127.9(6)	C(13)-C(14)-C(15)	113.7(8)

C(4)-C(3)-N(2)	105.5(6)	C(14)-C(15)-C(16)	123.5(8)
C(15)-C(16)-C(11)	118.2(6)	C(36)-C(31)-P(1)	116.9(3)
C(31)-P(1)-C(21)	104.0(2)	C(32)-C(31)-P(1)	124.0(4)
C(31)-P(1)-C(41)	102.1(2)	C(31)-C(32)-C(33)	119.7(5)
C(21)-P(1)-C(41)	102.8(2)	C(34)-C(33)-C(32)	121.3(5)
C(31)-P(1)-Cu(1)	116.42(14)	C(33)-C(34)-C(35)	118.9(5)
C(21)-P(1)-Cu(1)	116.47(15)	C(34)-C(35)-C(36)	120.2(5)
C(41)-P(1)-Cu(1)	113.12(15)	C(31)-C(36)-C(35)	120.8(4)
C(22)-C(21)-C(26)	118.6(5)	C(42)-C(41)-C(46)	119.0(5)
C(22)-C(21)-P(1)	123.9(4)	C(42)-C(41)-P(1)	123.3(4)
C(26)-C(21)-P(1)	117.6(3)	C(46)-C(41)-P(1)	117.7(4)
C(23)-C(22)-C(21)	120.6(5)	C(41)-C(42)-C(43)	120.2(6)
C(24)-C(23)-C(22)	119.9(5)	C(44)-C(43)-C(42)	119.9(6)
C(25)-C(24)-C(23)	120.7(5)	C(43)-C(44)-C(45)	120.3(6)
C(24)-C(25)-C(26)	119.6(6)	C(44)-C(45)-C(46)	119.9(6)
C(25)-C(26)-C(21)	120.6(5)	C(45)-C(46)-C(41)	120.6(6)
C(36)-C(31)-C(32)	119.1(5)		

Table S16. Torsion angles [°] for complex **1**.

C(5)-N(1)-N(2)-C(6)	-178.4(5)	P(1)-C(21)-C(22)-C(23)	-178.4(4)
Cu(1)-N(1)-N(2)-C(6)	-0.5(8)	C(21)-C(22)-C(23)-C(24)	-0.5(8)
C(5)-N(1)-N(2)-C(3)	0.2(5)	C(22)-C(23)-C(24)-C(25)	-0.3(9)
Cu(1)-N(1)-N(2)-C(3)	178.0(4)	C(23)-C(24)-C(25)-C(26)	1.2(10)
N(1)-N(2)-C(3)-C(4)	0.1(6)	C(24)-C(25)-C(26)-C(21)	-1.3(9)
C(6)-N(2)-C(3)-C(4)	178.5(6)	C(22)-C(21)-C(26)-C(25)	0.5(8)
N(2)-C(3)-C(4)-C(5)	-0.3(5)	P(1)-C(21)-C(26)-C(25)	179.5(4)
N(2)-N(1)-C(5)-C(4)	-0.3(5)	C(21)-P(1)-C(31)-C(36)	-165.0(4)
Cu(1)-N(1)-C(5)-C(4)	-178.9(3)	C(41)-P(1)-C(31)-C(36)	88.3(4)
N(2)-N(1)-C(5)-C(11)	177.5(4)	Cu(1)-P(1)-C(31)-C(36)	-35.4(4)
Cu(1)-N(1)-C(5)-C(11)	-1.0(5)	C(21)-P(1)-C(31)-C(32)	17.9(5)
C(3)-C(4)-C(5)-N(1)	0.4(5)	C(41)-P(1)-C(31)-C(32)	-88.9(5)
C(3)-C(4)-C(5)-C(11)	-177.2(5)	Cu(1)-P(1)-C(31)-C(32)	147.4(4)
N(1)-C(5)-C(11)-N(12)	-2.0(6)	C(36)-C(31)-C(32)-C(33)	-1.4(8)
C(4)-C(5)-C(11)-N(12)	175.4(4)	P(1)-C(31)-C(32)-C(33)	175.7(5)
N(1)-C(5)-C(11)-C(16)	179.3(4)	C(31)-C(32)-C(33)-C(34)	0.0(10)
C(4)-C(5)-C(11)-C(16)	-3.3(8)	C(32)-C(33)-C(34)-C(35)	0.1(10)
C(16)-C(11)-N(12)-C(13)	0.4(6)	C(33)-C(34)-C(35)-C(36)	1.1(9)
C(5)-C(11)-N(12)-C(13)	-178.3(4)	C(32)-C(31)-C(36)-C(35)	2.6(8)
C(16)-C(11)-N(12)-Cu(1)	-177.3(3)	P(1)-C(31)-C(36)-C(35)	-174.7(4)
C(5)-C(11)-N(12)-Cu(1)	4.0(5)	C(34)-C(35)-C(36)-C(31)	-2.5(8)
C(11)-N(12)-C(13)-C(14)	0.9(9)	C(31)-P(1)-C(41)-C(42)	15.8(5)
Cu(1)-N(12)-C(13)-C(14)	178.3(5)	C(21)-P(1)-C(41)-C(42)	-91.8(5)
N(12)-C(13)-C(14)-C(15)	-2.1(10)	Cu(1)-P(1)-C(41)-C(42)	141.7(4)
C(13)-C(14)-C(15)-C(16)	2.1(9)	C(31)-P(1)-C(41)-C(46)	-163.7(4)
C(14)-C(15)-C(16)-C(11)	-1.0(9)	C(21)-P(1)-C(41)-C(46)	88.7(4)
N(12)-C(11)-C(16)-C(15)	-0.4(7)	Cu(1)-P(1)-C(41)-C(46)	-37.8(4)
C(5)-C(11)-C(16)-C(15)	178.2(5)	C(46)-C(41)-C(42)-C(43)	0.3(8)
C(31)-P(1)-C(21)-C(22)	-86.2(4)	P(1)-C(41)-C(42)-C(43)	-179.3(5)
C(41)-P(1)-C(21)-C(22)	20.0(5)	C(41)-C(42)-C(43)-C(44)	0.5(10)
Cu(1)-P(1)-C(21)-C(22)	144.3(4)	C(42)-C(43)-C(44)-C(45)	-1.3(11)
C(31)-P(1)-C(21)-C(26)	95.0(4)	C(43)-C(44)-C(45)-C(46)	1.4(10)

C(41)-P(1)-C(21)-C(26)	-158.9(4)	C(44)-C(45)-C(46)-C(41)	-0.7(9)
Cu(1)-P(1)-C(21)-C(26)	-34.6(4)	C(42)-C(41)-C(46)-C(45)	-0.2(8)
C(26)-C(21)-C(22)-C(23)	0.4(7)	P(1)-C(41)-C(46)-C(45)	179.4(5)

Table S17. Crystal data and structure refinement for complex **2**.

Empirical formula	C ₃₂ H ₂₆ CuIN ₃ P
Formula weight	673.97
Temperature	200(2) K
Wavelength	0.71073 Å
Crystal system	Monoclinic
Space group	C2/c
Unit cell dimensions	a = 25.4203(15) Å b = 9.3752(5) Å c = 24.4816(16) Å β = 91.257(2)°
Volume	5833.1(6) Å ³
Z	8
Density (calculated)	1.535 Mg/m ³
Absorption coefficient	1.888 mm ⁻¹
F(000)	2688
Crystal size	0.300 x 0.200 x 0.080 mm ³
Theta range for data collection	1.603 to 29.218°.
Index ranges	-34 ≤ h ≤ 34, -8 ≤ k ≤ 12, -33 ≤ l ≤ 33
Reflections collected	33330
Independent reflections	7848 [R(int) = 0.0579]
Completeness to theta = 25.242°	99.8 %
Absorption correction	Semi-empirical from equivalents
Max. and min. transmission	0.7458 and 0.5513
Refinement method	Full-matrix least-squares on F ²
Data / restraints / parameters	7848 / 0 / 343
Goodness-of-fit on F ²	1.128
Final R indices [I > 2σ(I)]	R1 = 0.0550, wR2 = 0.1102
R indices (all data)	R1 = 0.0778, wR2 = 0.1198
Extinction coefficient	n/a
Largest diff. peak and hole	1.804 and -1.043 e.Å ⁻³

Table S18. Bond lengths [Å] and angles [°] for complex **2**.

Cu(1)-N(1)	2.062(3)	N(2)-C(3)	1.356(5)
Cu(1)-N(12)	2.116(3)	N(2)-C(6)	1.436(5)
Cu(1)-P(1)	2.1968(11)	C(3)-C(4)	1.367(6)
Cu(1)-I(1)	2.6127(6)	C(4)-C(5)	1.392(6)
N(1)-C(5)	1.345(5)	C(5)-C(12)	1.463(6)
N(1)-N(2)	1.351(5)	C(6)-C(7)	1.379(6)
C(6)-C(11)	1.382(6)	C(22)-C(23)	1.398(8)
C(7)-C(8)	1.395(6)	C(23)-C(24)	1.367(9)
C(8)-C(9)	1.375(7)	C(24)-C(25)	1.376(9)
C(9)-C(10)	1.369(8)	C(25)-C(26)	1.393(7)
C(10)-C(11)	1.396(7)	C(31)-C(32)	1.379(7)
C(12)-N(12)	1.346(5)	C(31)-C(36)	1.393(6)
C(12)-C(16)	1.396(5)	C(32)-C(33)	1.375(8)
N(12)-C(13)	1.345(5)	C(33)-C(34)	1.372(9)
C(13)-C(14)	1.387(6)	C(34)-C(35)	1.369(9)
C(14)-C(15)	1.375(7)	C(35)-C(36)	1.389(8)
C(15)-C(16)	1.390(6)	C(41)-C(46)	1.381(7)
P(1)-C(41)	1.822(4)	C(41)-C(42)	1.383(7)
P(1)-C(31)	1.831(5)	C(42)-C(43)	1.393(7)
P(1)-C(21)	1.834(4)	C(43)-C(44)	1.367(10)
C(21)-C(22)	1.379(6)	C(44)-C(45)	1.363(10)
C(21)-C(26)	1.382(6)	C(45)-C(46)	1.394(7)
N(1)-Cu(1)-N(12)	78.32(13)	C(7)-C(6)-C(11)	121.4(4)
N(1)-Cu(1)-P(1)	120.58(9)	C(7)-C(6)-N(2)	119.3(4)
N(12)-Cu(1)-P(1)	120.43(10)	C(11)-C(6)-N(2)	119.3(4)
N(1)-Cu(1)-I(1)	112.52(9)	C(6)-C(7)-C(8)	119.0(4)
N(12)-Cu(1)-I(1)	102.98(10)	C(9)-C(8)-C(7)	120.3(5)
P(1)-Cu(1)-I(1)	115.60(4)	C(10)-C(9)-C(8)	120.0(4)
C(5)-N(1)-N(2)	105.0(3)	C(9)-C(10)-C(11)	121.0(5)
C(5)-N(1)-Cu(1)	115.1(3)	C(6)-C(11)-C(10)	118.4(5)
N(2)-N(1)-Cu(1)	139.0(2)	N(12)-C(12)-C(16)	122.3(4)

N(1)-N(2)-C(3)	111.5(3)	N(12)-C(12)-C(5)	114.8(3)
N(1)-N(2)-C(6)	119.8(3)	C(16)-C(12)-C(5)	122.8(4)
C(3)-N(2)-C(6)	128.7(4)	C(13)-N(12)-C(12)	118.2(3)
N(2)-C(3)-C(4)	107.1(4)	C(13)-N(12)-Cu(1)	127.1(3)
C(3)-C(4)-C(5)	105.6(4)	C(12)-N(12)-Cu(1)	114.5(3)
N(1)-C(5)-C(4)	110.8(4)	N(12)-C(13)-C(14)	123.0(4)
N(1)-C(5)-C(12)	116.7(3)	C(15)-C(14)-C(13)	118.3(4)
C(4)-C(5)-C(12)	132.5(4)	C(14)-C(15)-C(16)	120.0(4)
C(15)-C(16)-C(12)	118.1(4)	C(36)-C(31)-P(1)	122.4(4)
C(41)-P(1)-C(31)	101.47(19)	C(33)-C(32)-C(31)	120.2(5)
C(41)-P(1)-Cu(1)	117.21(15)	C(34)-C(33)-C(32)	121.3(6)
C(31)-P(1)-Cu(1)	118.23(15)	C(35)-C(34)-C(33)	119.4(5)
C(21)-P(1)-Cu(1)	109.66(13)	C(34)-C(35)-C(36)	119.9(5)
C(22)-C(21)-C(26)	118.9(4)	C(35)-C(36)-C(31)	120.7(5)
C(22)-C(21)-P(1)	124.1(4)	C(46)-C(41)-C(42)	118.8(4)
C(26)-C(21)-P(1)	116.9(3)	C(46)-C(41)-P(1)	124.3(4)
C(21)-C(22)-C(23)	119.6(5)	C(42)-C(41)-P(1)	116.9(4)
C(24)-C(23)-C(22)	121.0(5)	C(41)-C(42)-C(43)	120.4(6)
C(23)-C(24)-C(25)	119.9(5)	C(44)-C(43)-C(42)	120.4(6)
C(24)-C(25)-C(26)	119.2(6)	C(45)-C(44)-C(43)	119.4(5)
C(21)-C(26)-C(25)	121.4(5)	C(44)-C(45)-C(46)	121.1(6)
C(32)-C(31)-C(36)	118.4(5)	C(41)-C(46)-C(45)	119.8(6)
C(32)-C(31)-P(1)	119.2(4)		

Table S19. Torsion angles [°] for complex **2**.

C(5)-N(1)-N(2)-C(3)	0.5(4)	N(2)-N(1)-C(5)-C(12)	179.2(3)
Cu(1)-N(1)-N(2)-C(3)	168.7(3)	Cu(1)-N(1)-C(5)-C(12)	7.7(4)
C(5)-N(1)-N(2)-C(6)	177.8(3)	C(3)-C(4)-C(5)-N(1)	0.0(5)
Cu(1)-N(1)-N(2)-C(6)	-14.0(6)	C(3)-C(4)-C(5)-C(12)	-179.4(4)
N(1)-N(2)-C(3)-C(4)	-0.5(5)	N(1)-N(2)-C(6)-C(7)	-39.9(5)
C(6)-N(2)-C(3)-C(4)	-177.5(4)	C(3)-N(2)-C(6)-C(7)	136.8(5)
N(2)-C(3)-C(4)-C(5)	0.3(5)	N(1)-N(2)-C(6)-C(11)	141.3(4)
N(2)-N(1)-C(5)-C(4)	-0.4(4)	C(3)-N(2)-C(6)-C(11)	-42.0(6)
Cu(1)-N(1)-C(5)-C(4)	-171.8(3)	C(11)-C(6)-C(7)-C(8)	-1.4(7)
N(2)-C(6)-C(7)-C(8)	179.9(4)	P(1)-C(21)-C(26)-C(25)	176.2(4)
C(6)-C(7)-C(8)-C(9)	0.7(8)	C(24)-C(25)-C(26)-C(21)	0.2(8)
C(7)-C(8)-C(9)-C(10)	0.4(8)	C(41)-P(1)-C(31)-C(32)	-145.3(4)
C(8)-C(9)-C(10)-C(11)	-0.8(9)	C(21)-P(1)-C(31)-C(32)	106.6(4)
C(7)-C(6)-C(11)-C(10)	1.0(8)	Cu(1)-P(1)-C(31)-C(32)	-15.6(5)
N(2)-C(6)-C(11)-C(10)	179.8(5)	C(41)-P(1)-C(31)-C(36)	35.1(5)
C(9)-C(10)-C(11)-C(6)	0.1(9)	C(21)-P(1)-C(31)-C(36)	-73.0(5)
N(1)-C(5)-C(12)-N(12)	-7.5(5)	Cu(1)-P(1)-C(31)-C(36)	164.8(4)
C(4)-C(5)-C(12)-N(12)	171.9(4)	C(36)-C(31)-C(32)-C(33)	-0.6(8)
N(1)-C(5)-C(12)-C(16)	171.8(4)	P(1)-C(31)-C(32)-C(33)	179.8(5)
C(4)-C(5)-C(12)-C(16)	-8.7(7)	C(31)-C(32)-C(33)-C(34)	1.5(10)
C(16)-C(12)-N(12)-C(13)	-0.5(6)	C(32)-C(33)-C(34)-C(35)	-1.6(11)
C(5)-C(12)-N(12)-C(13)	178.8(4)	C(33)-C(34)-C(35)-C(36)	0.9(11)
C(16)-C(12)-N(12)-Cu(1)	-175.8(3)	C(34)-C(35)-C(36)-C(31)	0.0(10)
C(5)-C(12)-N(12)-Cu(1)	3.6(4)	C(32)-C(31)-C(36)-C(35)	-0.1(9)
C(12)-N(12)-C(13)-C(14)	0.6(7)	P(1)-C(31)-C(36)-C(35)	179.5(5)
Cu(1)-N(12)-C(13)-C(14)	175.1(4)	C(31)-P(1)-C(41)-C(46)	-99.7(4)
N(12)-C(13)-C(14)-C(15)	0.0(7)	C(21)-P(1)-C(41)-C(46)	8.6(5)
C(13)-C(14)-C(15)-C(16)	-0.5(7)	Cu(1)-P(1)-C(41)-C(46)	130.0(4)
C(14)-C(15)-C(16)-C(12)	0.5(6)	C(31)-P(1)-C(41)-C(42)	78.4(4)
N(12)-C(12)-C(16)-C(15)	0.0(6)	C(21)-P(1)-C(41)-C(42)	-173.3(4)
C(5)-C(12)-C(16)-C(15)	-179.3(4)	Cu(1)-P(1)-C(41)-C(42)	-51.9(4)
C(41)-P(1)-C(21)-C(22)	-102.3(4)	C(46)-C(41)-C(42)-C(43)	3.5(8)

C(31)-P(1)-C(21)-C(22)	3.8(4)	P(1)-C(41)-C(42)-C(43)	-174.7(5)
Cu(1)-P(1)-C(21)-C(22)	131.5(4)	C(41)-C(42)-C(43)-C(44)	-1.2(9)
C(41)-P(1)-C(21)-C(26)	82.3(4)	C(42)-C(43)-C(44)-C(45)	-1.7(9)
C(31)-P(1)-C(21)-C(26)	-171.6(3)	C(43)-C(44)-C(45)-C(46)	2.2(9)
Cu(1)-P(1)-C(21)-C(26)	-44.0(4)	C(42)-C(41)-C(46)-C(45)	-3.0(8)
C(26)-C(21)-C(22)-C(23)	-0.6(7)	P(1)-C(41)-C(46)-C(45)	175.1(4)
P(1)-C(21)-C(22)-C(23)	-176.0(4)	C(44)-C(45)-C(46)-C(41)	0.1(8)
C(21)-C(22)-C(23)-C(24)	-0.1(9)		
C(22)-C(23)-C(24)-C(25)	0.8(9)		
C(23)-C(24)-C(25)-C(26)	-0.9(9)		
C(22)-C(21)-C(26)-C(25)	0.5(7)		
